Experimental results on the performance of Optical Spatial Modulation systems

Enrique Poves, Wasiu Popoola, Harald Haas and John Thompson
Institute for Digital Communications
University of Edinburgh
EH9 3JL Edinburgh, UK
Email: {e.poves, w.popoola, h.haas, john.thompson}@ed.ac.uk

Daniel Cárdenas
Universidad San Francisco de Quito
M103A, Quito, Ecuador
Email: dcardenas@usfq.edu.ec

***Abstract*—Spatial Modulation (SM) is a relatively new technique to include information bits in the spatial domain, combining multiple-input multiple-output (MIMO) and digital modulation techniques. The increase on the overall data rate is achieved by activating only one transmitter at any time, whereas the index of the active emitter represents data bits. At the receiver side the active transmitter index is estimated based on the channel gain for the different paths. In this work we show the behaviour of an optical SM wireless communications system. A fully operative test system consisting of four transmitters and one receiver has been implemented and tests have been conducted to obtain the symbol error rate (SER) for different link distances. Results show the strong relation between the error rate achieved and the relative channel gain differences between all channels rather than the individual signal-to-noise ratio (SNR).**

***Index Terms*—Spatial Modulation (SM), Optical Spatial Modulation (OSM), Optical Wireless Communications (OWC), multiple-input multiple-output (MIMO), Direct Detection.**

I. Introduction

Technology improvements on solid state lighting devices over the last decade have attracted attention from both academy and industry on visual light communications (VLC). The availability of high power LEDs (light emitting diodes) for lighting and their advantages in terms of regulation, cost and reliability over traditional incandescent lamps have opened a new field for optical wireless communications. Lighting LEDs can be based on blue emitters and yellow phosphor or on a combination of red, green and blue emitters to produce white light. The former have narrow bandwidth for data transmission due to the slow temporal response of the phosphor compared to the LED response, although this effect can be mitigated by using optical filters in the receiver. RGB LEDs present an improved frequency response, but the modulation process is more complex to avoid color flickering. As opposed to traditional infrared optical links power budget is no longer an issue as visible light LEDs provide higher output to fulfill their illumination purposes. Therefore most efforts are oriented towards increasing the maximum achievable data rate by overcoming the switching characteristics of LEDs, which are particularly limited for those phosphor-based.

Traditionally, single-carrier pulsed modulation techniques such as on-off keying (OOK) or pulse-position modulation (PPM) have been used in optical wireless [1]. The latter offers high power efficiency and low implementation effort, although the performance is severely affected by multipath induced intersymbol interference and data rate is limited. Alternatively, multiple-subcarriers modulation techniques commonly used in radiofrequency systems, especially orthogonal frequency-division multiplexing (OFDM), have been applied to the optical domain and extensively tested [2]. They offer good bandwidth efficiency and are robust against multipath propagation and intersymbol interference, but provide poor power efficiency. Lastly, in the late years the application of multiple-input multiple-output (MIMO) techniques to optical communications have been proposed as a way to obtain high data rate systems [3].

Spatial Modulation (SM) was recently proposed as an alternative MIMO system, and can also be applied to optical wireless communications [4], [5]. In an Optical SM system multiple transmitters are installed but only one is active at any given time. The active emitter is determined by the incoming data stream, and it can be estimated on the receiver side by applying the maximum likelihood principle. This way the average power efficiency is improved and the data rate enhanced. Simulations show that system performance suffers a strong degradation when geometry differences between emitters and receivers decrease, resulting in highly correlated optical channels [6], although this effect can be improved by increasing the number of receiver units and applying channel coding techniques.

In this paper a demonstrator for OSM is presented and the experimental results discussed. Four transmitting units and one receiver has been used to study the performance of the system for different link distances. Symbol error rate measurements have been conducted at different link distances, showing a strong dependence on the channel gain for a single receiver.

The rest of the paper is organized as follows. Section II briefly describes the optical spatial modulation technique and the encoding procedure. Section III details the implementation of the system used for the tests and the characteristics of both hardware and software subsystems. Tests' results are presented and discussed in section IV, and conclusions provided in section V.

978-1-4673-1881-5/12/$31.00 ©2012 IEEE

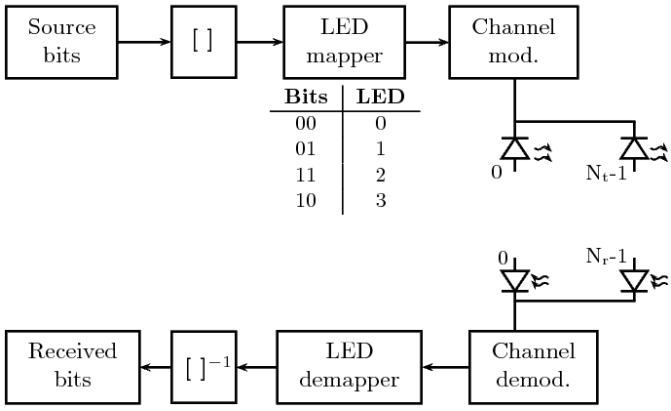

Fig. 1. OSM transmitter model

II. Optical Spatial Modulation

The block model of a generic OSM system is shown in Fig. 1, consisting of N_t transmitting and N_r receiving units, i.e. LEDs and photodiodes respectively. Data encoding is performed by grouping together each $\log_2(N_t)$ bits from the source stream and then mapping them to LED indexes (symbols). At any given time, the selected LED will send a predefined signal, while all other units remain idle. In OSM the emitted intensity level carries no information and can be chosen to optimize the power efficiency of the system. An in-depth review of the system model can be found in [6]. At the receiver side, the photodiode converts the optical signal to an electrical signal and applies the optimal SM detector [7] to estimate the active transmit unit index. This recovered symbol is then used to retrieve the data bits by reversing the mapping process with the same mapping table as originally used in the transmitter. It has been reported that the error performance of OSM systems depends on the locations and the directions of the transmit and receive units, and that it deteriorates due to the optical channel correlation [5].

The system implemented uses $N_t = 4$ emitters and $N_r = 1$ receiver. The active LED mapping from the incoming source bitstream is shown in table I. Assuming emitters' position ensure different channel gain for each link, simple decision based on amplitude can be made on the receiver. However, the high correlation of the channel paths, with transmit units only a few centimeters apart, and the lack of receive diversity caused by a single receiver affects the overall performance of OSM in these conditions.

TABLE I
LED mapping

Input bits	LED index
00	0
01	1
11	2
10	3

With no receive diversity and incoherent detection, the estimation of the sent symbols is to be based on the different channel gain [8] from each transmitter. For the test setup a line-of-sight configuration was selected, minimizing the multipath contribution for all links on the receiver. Transmitted power is the same for all units, thus the optical power differences on the receiver depend only on the emission angle due to the narrow emitter's directivity, and the link distance from each LED.

The receiver electronics will be discussed later, but as AC coupling has been used to minimize ambient light-related problems return-to-zero (RZ) coding was chosen as the transmission format instead of a fixed intensity level. This way both low and high level signals are available on the receiver and the peak-to-peak amplitude can be computed for each symbol. By comparing this value with the expected average amplitude from each LED the active emitter can be estimated, and the incoming symbols decoded.

III. System Description

A. Design parameters

A test system has been developed to verify the behaviour of OSM in a real transmission environment. The design implements a fully operative OSM terminal with $N_t = 4$ and $N_r = 1$. It is based on a Xilinx's Virtex-6 FPGA ML605 Evaluation Kit [9] for quicker implementation, which includes an auxiliary board with an analog-to-digital converter. All signal manipulation is done by the FPGA in real time and only individual signals (sent bits, recovered bits and input signal's samples) are available to a computer for performance analysis and error probability characterization. Custom optical front-ends have been developed to perform the optical data transmission and reception.

Data rate is desired to use the maximum bandwidth available for phosphor-based white LEDs, which studies show is around 20 MHz [10]. Due to the particular restrictions on the selected platform the system's clock and data frequencies have been chosen as follows:

- Symbol rate $R_s = 9.216$ Mbaud
- Bit rate $R_b = 18.432$ Mbit/s
- Sampling frequency $f_s = 73.728$ MHz, resulting in 8 samples per symbol

As the intensity level emitted by the active LED carries no information in OSM systems a RZ code has been used instead of a fixed signal, except for the synchronization symbols. This channel modulation assures peak-to-peak amplitude values are available in the receiver and can be used in the decision process. Symbols are therefore transmitted as a low amplitude level (i.e. LED off) followed by a high level (i.e. LED on), both of duration half the symbol period ($T_s/2$). This permits the use of an AC-coupled receiver chain which helps mitigate the interference from external light sources, although the maximum achievable symbol rate is reduced to guarantee the LED can switch completely on and off during the symbol period.

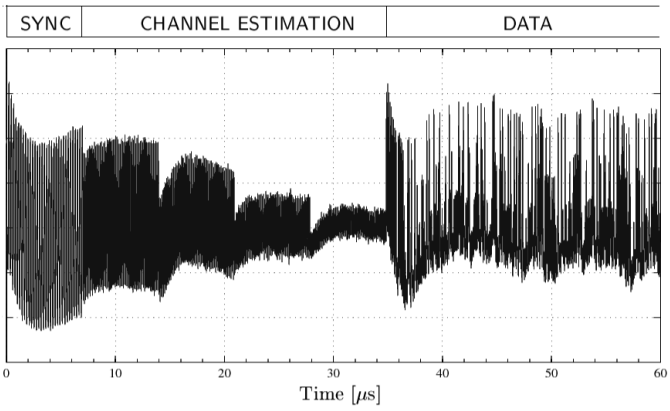

Fig. 2. Data frame and Received signal

B. Frame Organization

The data frame organization is shown in Fig. 2, along with the electrical signal on the receiver. A synchronization sequence (SYNC) is transmitted at the beginning of each frame. Symbols are coded as non-return-to-zero waveforms, thus violating the RZ coding premise, helping the receiver identify the start of a new frame. This sequence is formed by a series of 64 alternating on and off symbols which are only emitted by the first LED (namely LED0).

A channel estimation process is performed afterwards to enable the receiver evaluate the channel gain for each link. All four emitters (LED0 to LED3) are enabled sequentially to send a predefined pattern consisting of 64 RZ mark symbols. As the gain is different for each channel path, different amplitude levels will be detected at the receiver from each LED –as observed in Fig. 2. Average amplitude is calculated for each link and stored in the receiver, and the value for each channel will be used as the basis for the decision making process. Finally, the frame includes 2^{16} data bits that are encoded to symbols and sent by the selected LED as shown in table I.

C. Transmitter subsystem

The transmitter's software implemented in the FPGA board is based on a finite-state machine which loops between three states corresponding to the different fields within the data frame, i.e. synchronization, channel estimation and data transmission. Dedicated generators output the emitted signal (both RZ and NRZ waveforms), while the LEDs are individually enabled according to the current state and incoming data. Source data bits are generated by a 16-stage Fibonacci linear-feedback shift-register, producing a pseudo-random sequence of length 65,535 bits. This sequence is encoded as described in section II and used to enable the transmission from the appropriate LED.

High brightness 5 mm white LEDs (OVL5521 from Multicomp [11]) are used for the optical emission. These LEDs offer a high luminous output (18 cd at 20 mA) with a narrow full viewing angle (15°). Although this device admits pulsed currents up to 100 mA, the LED current has been adjusted to 45 mA to ensure it can be turned off completely within the symbol period considering the slow time response of the phosphor (fall times of 60 ns were measured). Each LED is driven by a bipolar transistor (ZTX450 from Diodes Inc.) controlled by the sent data signal coming from the FPGA interface.

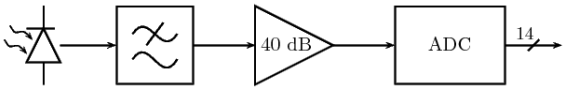

Fig. 3. Receiver schematics

D. Receiver subsystem

The receiver part consists of a 26 mm^2 silicon PIN photodiode (S6967 from Hamamatsu, with 50 MHz cut-off frequency and peak sensitivity at 900 nm [12]) and a transimpedance amplifier (AD8015 from Analog Devices), followed by a second order low-pass filter and a 40 dB amplifier chain (see Fig. 3). The resulting signal is then passed to a 14-bit analog-to-digital converter (ADS62P49 from Texas Instruments), and its output registered by the FPGA program at the specified sampling rate. The ADC board is AC-coupled and has a differential input voltage range of only 2 V_{pp} which may result in signal clipping for very short link distances, increasing the number of decision errors. The optical receiver also includes a lens with 3 cm focal length to concentrate the incoming light on the sensitive area, and a 460±30 nm interference filter to select blue wavelengths and avoid problems induced by the low temporal response of the yellow phosphor of the LED.

The receiver chain has been designed to provide an almost flat response ranging from 400 kHz to 20 MHz, so most optical interference from other light sources is attenuated while maintaining the signal frequencies. Electrical noise analysis was performed to obtain an optical noise equivalent power at the receiver to refer the signal-to-noise measurements, resulting in $N_{eq} = -40$ dBm.

The software receiver firstly tracks the synchronization acquisition by detecting the SYNC field. Input samples are reduced to their most significant bit (sign bit) and the expected pattern is seeked for groups of 16 samples (2 symbols) at constantly spaced intervals. Once all ocurrences have been detected the channel estimation series are analyzed. Maximum and minimum sample values are selected for each symbol duration (8 samples), and cumulative moving average is computed to obtain the channel's average peak-to-peak amplitude. This value is stored for each LED so it can be used as a threshold during the data decoding process. Lastly, data is processed in a similar way obtaining the amplitude for each symbol received. The channel gain is assumed to be constant (or varying slowly) during the frame reception, so that all symbols emitted by any given LED will have similar amplitude values on the receiver. Therefore the decision on the received symbol is made based on the minimum distance from

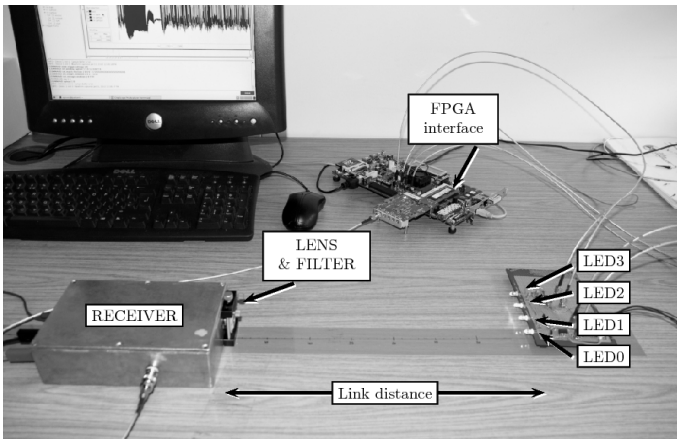

Fig. 4. Test setup

the current symbol's peak-to-peak amplitude to the thresholds stored for all channels.

IV. Experimental Results and Discussion

Tests have been conducted on the system to assess the symbol error rate performance of OSM. The pseudo-random symbol sequence generated in the transmitter was passed from the FPGA to a computer, and stored along with the recovered data symbol sequence to obtain error statistics. Signal samples were also made available, and a MATLAB-based software decoder has been used to verify the decision process was running correctly.

The FPGA interface's memory size presented a limitation of 131,072 data samples, thus reducing the number of symbols available for the SER calculations. As 16,000 symbols were captured each time, the minimum detectable error rate is 6×10^{-5}. Multiple runs were performed for each configuration, and the error rate presented in this paper corresponds to the average of all the values obtained.

The test configuration is shown in Fig. 4. Receiver unit is aligned to LED0 emitter to ensure different channel gains for each link, and all emitters are spaced 2.5 cm in the perpendicular direction. Measurements were taken for link distances ranging from 25 to 60 cm, as some of the LEDs would not be detected at shorter link distances due to their narrow emission angle (particularly LED3, furthest from the link reference), and longer distances suffer from strong degradation of the signal-to-noise ratio (SNR) differences as the channel gains reach similar values.

Signal power measurements were taken for each LED to assess the dependence of the error rate on the link distance and transmitter-receiver alignment, and obtain the signal-to-noise ratio. Measured values are presented in Fig 5(a). It can be seen that optical power from LED2 and LED3 show different tendencies because of the higher angle from these emitters to the receiver. The narrow emission angle of the LED leads to a weak signal being detected for short link distances. Also a small misalignment for LED1 can be observed, leading to weaker values that those of LED2 for long distances.

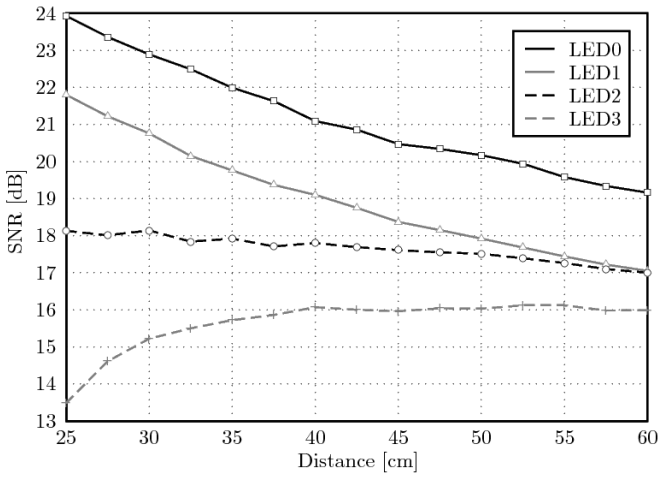

(a) SNR vs link distance

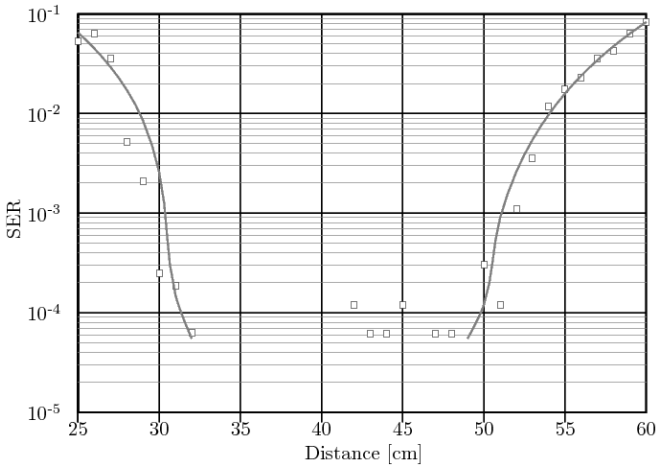

(b) SER vs link distance

Fig. 5. Experimental results

Measured SER is shown in Fig. 5(b), where dots represent actual measurement values (taken at 1 cm intervals) and curve fitting results for the near and far regions are plot as continuous lines. Different tendencies can be observed for short and long link distances, and will be discussed individually.

A detailed data analysis shows that for distances up to 33 cm most errors occur for symbols 2 and 3 (transmitted by LED3 and LED2 respectively). Given their position on the further end of the transmitter board, these LEDs fit only a small portion of the emitted optical power into the receiver, resulting in low SNR values that lead to more errors in the active transmitter estimation (up to 20% of symbols transmitted).

On the other end, for distances above 50 cm most errors happen for LED1 and LED2, although all channels are affected and partial error statistics rise quickly. The misalignment of LED1 causes the errors on LED1 and LED2 as the optical power received from them reaches similar levels. Long distance links reduce the channel gain differences and the SNR takes closer values (as seen in Fig. 5(a)), resulting in small differences between the channel thresholds in the decision

process and more erroneous decisions.

In the medium range distances, from 33 to 50 cm, only isolated errors were present. Values shown represent to just 1 or 2 errors within the captured data stream (corresponding to SER of 6.2×10^{-5} and 1.2×10^{-4} respectively). It can be seen that in this range no errors were detected for most of link distances.

These results show that in a OSM system with $N_r = 1$ receiver unit, SER is not only related to each channel's absolute SNR values but to the difference between all of them. Singular or no errors will be obtained if the channel gains lead to clear well-spaced SNR values on the receiver. Therefore the maximum number of transmitters that can be accommodated in an OSM system with a single receiver will be related to the relative channel gain differences rather than to the particular individual gains.

Received signal was also affected by AC-wandering, which caused part of the errors detected. During the reception of the channel estimation field the received signal maintains a steady DC component, while it is changing during the data acquisition. This leads to slight differences between the expected thresholds and the actual symbol's peak-to-peak amplitudes, resulting in wrong decisions when the symbol thresholds are close (i.e. for long link distances).

The low optical power of the LEDs used for transmission (18 cd) imposes a limitation on the maximum link distance that can be achieved with this test system. However LED lighting devices of over 500 cd are commercially available, expanding the maximum link distance to more than 4 meters. This range would be enough for the system to work in a medium-sized room providing a data broadcast channel in addition to the illumination.

V. Conclusions and future work

A fully operative autonomous system for optical spatial modulation has been implemented and tested, using $N_t = 4$ emitter units and $N_r = 1$ receiver. Commercial off-the-shelf components have been used for the design. Data is encoded in the spatial domain only, with a data rate of 18 Mbit/s which is only limited by the LED's temporal response. Tests have been performed to characterize the signal-to-noise ratio on the receiver, confirming the influence of the transmission angle due to the narrow viewing angle of the LEDs. Symbol error rate has been also measured for different link distances, showing the strong relation with the signal-to-noise ratio differences when all channel paths are highly correlated. The OSM technique has been demostrated with error-free transmissions when the channel gains for all different channel paths can be clearly identified.

The system can be easily upgraded to accomodate a different number of receivers and/or transmitters. Further work is being done to use multiple receiver units, implementing diversity on the receiver. This will provide different link paths with lower correlation and will improve the decision process, helping achieve lower SER for longer distances. Also, the system is being prepared to accommodate a larger number of transmitter units, which will allow higher data transmission rates.

Acknowledgements

Authors gratefully acknowledge support for this work from the UK Engineering and Physical Sciences Research Council (EPSRC) under grant EP/I013539/1.

References

[1] T. Komine and M. Nakagawa. Fundamental analysis for visible-light communication system using LED lights. *Consumer Electronics, IEEE Transactions on*, 50(1):100–107, February 2004.

[2] H. Elgala, R. Mesleh, and H. Haas. Practical considerations for indoor wireless optical system implementation using OFDM. In *Telecommunications, 2009. ConTEL 2009. 10th International Conference on*, pages 25–29, June 2009.

[3] L. Zeng, D. O'Brien, H. L. Minh, G. E. Faulkner, K. Lee, D. Jung, Y. Oh, and E. T. Won. High data rate multiple input multiple output (MIMO) optical wireless communications using white LED lighting. *Selected Areas in Communications, IEEE Journal on*, 27(9):1654–1662, December 2009.

[4] R. Mesleh, H. Haas, C. W. Ahn, and S. Yun. Spatial modulation - a new low complexity spectral efficiency enhancing technique. In *Communications and Networking in China, 2006. ChinaCom '06. First International Conference on*, pages 1–5, October 2006.

[5] R. Mesleh, R. Mehmood, H. Elgala, and H. Haas. Indoor MIMO optical wireless communication using spatial modulation. In *Communications (ICC), 2010 IEEE International Conference on*, pages 1 –5, May 2010.

[6] R. Mesleh, H. Elgala, and H. Haas. Optical spatial modulation. *Optical Communications and Networking, IEEE/OSA Journal of*, 3(3):234–244, March 2011.

[7] J. Jeganathan, A. Ghrayeb, and L. Szczecinski. Spatial modulation: optimal detection and performance analysis. *Communications Letters, IEEE*, 12(8):545 –547, August 2008.

[8] J. M. Kahn and J. R. Barry. Wireless infrared communications. *Proceedings of the IEEE*, 85(2):265–298, February 1997.

[9] Xilinx Inc. Virtex-6 FPGA ML605 evaluation kit - user guide. http://www.xilinx.com.

[10] J. Grubor, S. Randel, K.D. Langer, and J.W. Walewski. Bandwidth-efficient indoor optical wireless communications with white light-emitting diodes. In *Communication Systems, Networks and Digital Signal Processing, 2008. CNSDSP 2008. 6th International Symposium on*, pages 165–169, July 2008.

[11] Multicomp. Datasheet: OVL5521 5.0 mm round LED lamp.

[12] Hamamatsu. Datasheet: S6967 si PIN photodiodes. Available at http://www.hamamatsu.com.